Direct Feedback Control of Gas-Phase Laser-Induced Deposition

J. L. Maxwell[1], J. Pegna, D. Messia, D. DeAngelis

Center for Integrated Electronics and Integrated Manufacturing, Rensselaer Polytechnic Institute, Troy, New York 12180-3590
Tel: (518) 276-6030, Fax: (518) 276-2623, email: pegnaj@rpi.edu.

Abstract: *Three-dimensional laser Chemical vapor deposition (3D-LCVD) or SALD, was used to prototype metallic and ceramic microstructures. Iron, nickel, and steel metal forms were grown from organic and halogen based precursors. Through the simultaneous use of multiple precursors, specific nickel-iron based alloys were produced. By observing the emission spectra during growth, a measure of the volumetric growth rate, was obtained. Direct, PID control of the process was then possible using the growth rate measurement as real-time feedback. Calibrated infrared photographs of evolving microstructures were taken at various wavelengths, giving a measure of the temperature gradient over the growth zone. While radiation contributes to heat losses at high temperatures, enhanced convection is the dominant heat transfer mechanism due to the small dimensions of the heated area. Enhanced growth rates, induced by convective flow, were also observed. The heat and mass transfer coefficients were determined for various processing conditions, and compare well with experimental data. Axi-symmetric rods may also be grown in both the kinetic and transport-limited regimes, and a systematic study of the precursor pressure and deposit temperature during growth yielded distinct growth regimes, influenced by the interplay of heat losses and diffusive transport.*

Keywords: *Solid Area Laser Deposition, Chemical Vapor Deposition, Graphite, Iron, Nickel, Nickel-Iron Alloys, PID Process Control.*

1. Current Affiliation: Institute for Micromanufacturing, Louisiana Tech University, Ruston, La 71270

1 INTRODUCTION

Laser-induced chemical vapor deposition (LCVD) has been explored extensively as a thin-film metallization tool. In contrast, three-dimensional laser chemical vapor deposition, 3D-LCVD (or SALD), is a mode of pyrolytic deposition where more elevated structures can be generated, as exemplified in figures 1, 2, and 3. Our interest in 3D-LCVD is in its use as a free-form rapid-prototyping tool for micro to milli-scale mechanical objects.

Past attempts at control of the 3D LCVD process have been for the most part open-loop, growth rates and required process conditions being estimated from empirical data. The purpose of this work was to determine a method for measuring and controlling the volumetric deposition rate during 3D-LCVD.

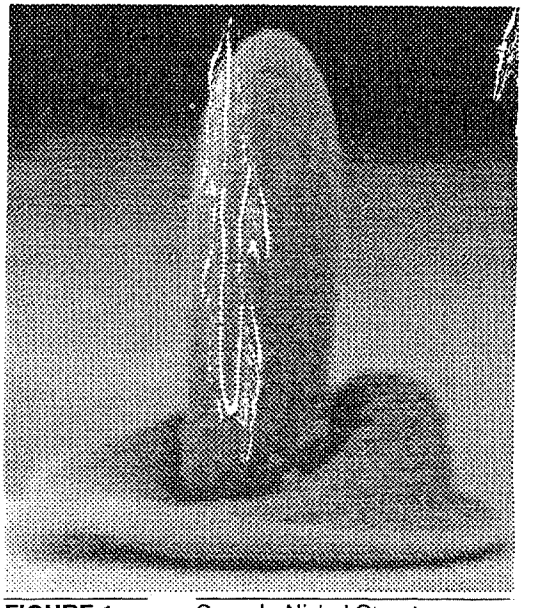

FIGURE 1. Sample Nickel Structure.

In this work, the volumetric growth rate was measured directly from the emission spectra associated with the pyrolytic reaction. This rate measurement was used to control the input power and instantaneous growth rates. Applications include control of laser direct writing over varying substrate topography, control of undesirable features in layered growth, and implementation of continuous 3-dimensional deposition.

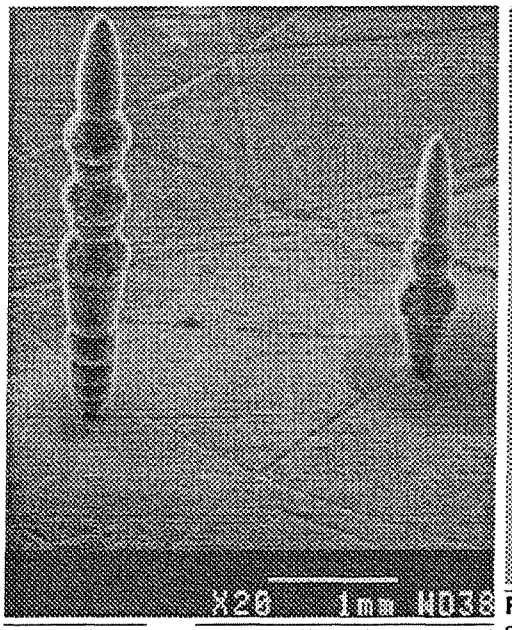

FIGURE 2. Sample Nickel-Iron alloyed structure.

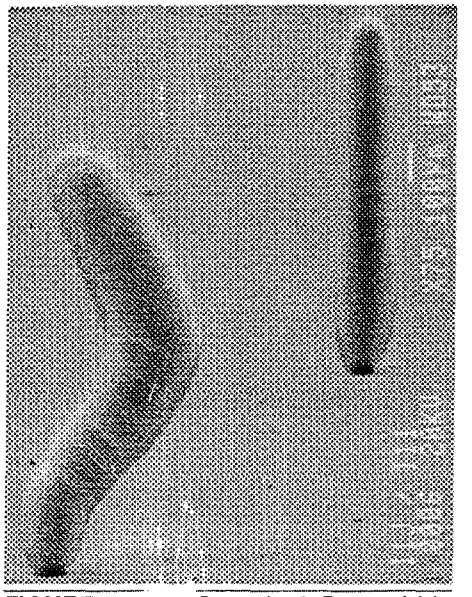

FIGURE 3. Sample 3-D graphitic structures.

Besides demonstrating the potential of 3D-LCVD for the prototyping of alloys, the purpose of the experiments was also to determine variations in final deposit compositions–so that the temperature changes during rod growth can be determined–as well as the difference in activation energies (Ea) of the iron and nickel carbonyl precursors. This result, however, will not be discussed within the scope of this paper. For more information on this subject, the reader is referred to [Maxwell et al., 1996].

2 EXPERIMENTAL

The 3D-LCVD reactor at Rensselaer consists of a custom quartz tube with a port for viewing and laser input. The chamber is connected to a pumping station via a gate valve. The vacuum chamber and gas-delivery system are enclosed within a ventilated hood for safety purposes.

Iron pentacarbonyl was delivered to the reaction chamber via an evaporator. In this experiment, the room-temperature vapor pressure of $Fe(CO)_5$ was used to fill the chamber. In most cases, the partial pressure of the precursor reached 20 mbar.

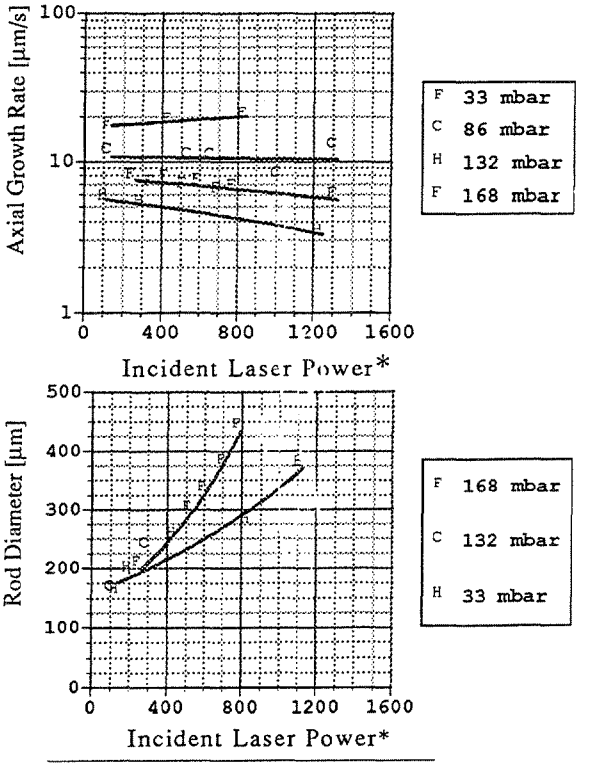

* Corrected for optical losses.

FIGURE 4. Nickel average axial growth rates and diameter vs. input power.

Both ethylene and nickel tetracarbonyl were metered into the reactor from commercial cylinders. For the growth of pyrolytic graphite, ethylene pressures of up to 930 mbar were employed. $Ni(CO)_4$ partial pressures of up to 250 mbar were possible. Iron pentacarbonyl was delivered to the reaction chamber via an evaporator. In these experiments, the room-temperature vapor pressure of $Fe(CO)_5$ was used to fill the chamber, i.e. 20 mbar.

The beam source was a Spectra Physics argon-ion laser, with a maximum output of 8 watts (multi-mode) at the 488/514 nm primary lines. At these wavelengths, iron and nickel have normal spectral reflectances of 65% and 52% respectively [Touloukian, 1970]. Gaussian spot radii of 25 μm ($1/e^2$) or greater were used throughout the experiments, and it was found that while the commencement of growth on the substrate depended greatly on the power density—requiring small spot sizes for the laser powers available— the 3-D, steady-state growth of rods was nearly unaffected by the beam waist over a distance several times the Rayleigh range (250 μm). The optical system consisted of a Newport 10x beam expander and 200 mm focal length CVI achromat. A long pass filter was used to block the UV laser lines below 420 nm.

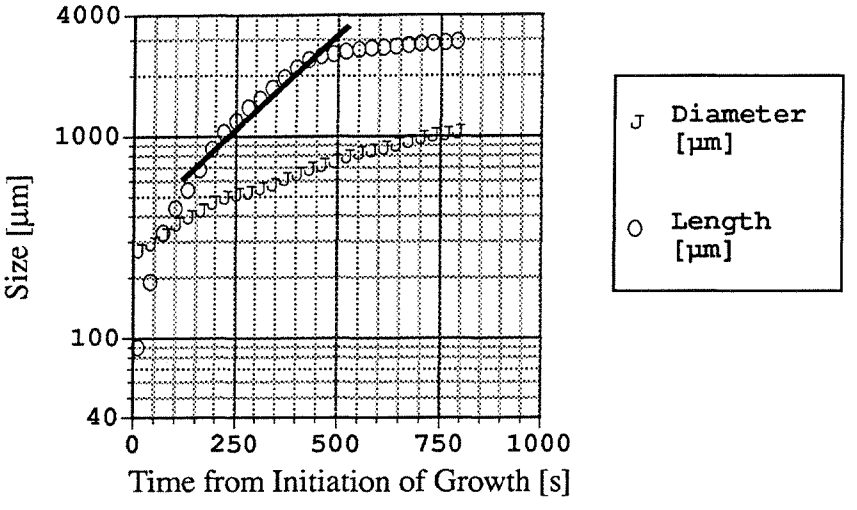

FIGURE 5. Nickel rod length and mid-length diameter vs. time

A silicon photodetector, covered with narrowband filters, was mounted to one of the chamber windows, at a distance roughly 200 mm from the sample. Using a two-decade pre-amplifier, the sensor could measure emissions as small as 0.25 mW at the substrate (at 656 nm). In this arrangement, the sensor had a time response on the order of milliseconds; however, the amplifier was heavily filtered with a time-constant of approximately 1/30 s. The amplified signal was recorded by an Omega Nubus data acquisition system, with a typical sample period of 0.05-0.10 seconds, and was later time averaged as needed for real-time control. Proportional-Integral-Derivative (PID) Control of the laser power was implemented using Omega Workbench™ software with output to the LCD retarder mentioned previously.

For analysis of the sample composition, both Auger electron spectroscopy (PHI 545C Scanning Auger Microprobe) and an electron microprobe (Geol Superprobe 733) were employed. Prior to the microprobe analysis, the samples were sectioned, polished, and lightly etched in a Kalling's solution, a mixture of isopropyl alcohol, HCL, and $CuCl_2$.

3 RESULTS AND DISCUSSION

3.1 NI GROWTH

Ni(CO)4 vapor pressures ranged from 25 to 200 mbar throughout the experiment, and rods could be initiated at pressures of less than 25 mbar. At similar partial pressures, the axial growth rate was higher than that of the ethylene-grown structures, exceeding 18 mm/s at the highest powers. Surprisingly, preliminary results for the axial growth rate show that the highest normal growth rates values were obtained at the lowest pressures, as indicated in Figure 4 (top.)

As for steady state diameter, experimental results recorded in Figure 4 (bottom) indicate that increasing pressure broadens the rod, just as for ethylene at partial pressures below 200 mbar. Interestingly, for all Ni(CO)4 pressures, the diameters approach a non-zero asymptotic diameter, approximately 60 mm wide. One possible implication is that, for these pressures, it may not be possible to grow narrow Ni structures thinner than 100 mm, thereby limiting the resolution of the process. Further experiments at very low laser powers (<100 mW) and small beam waist diameter are needed to confirm this phenomenon.

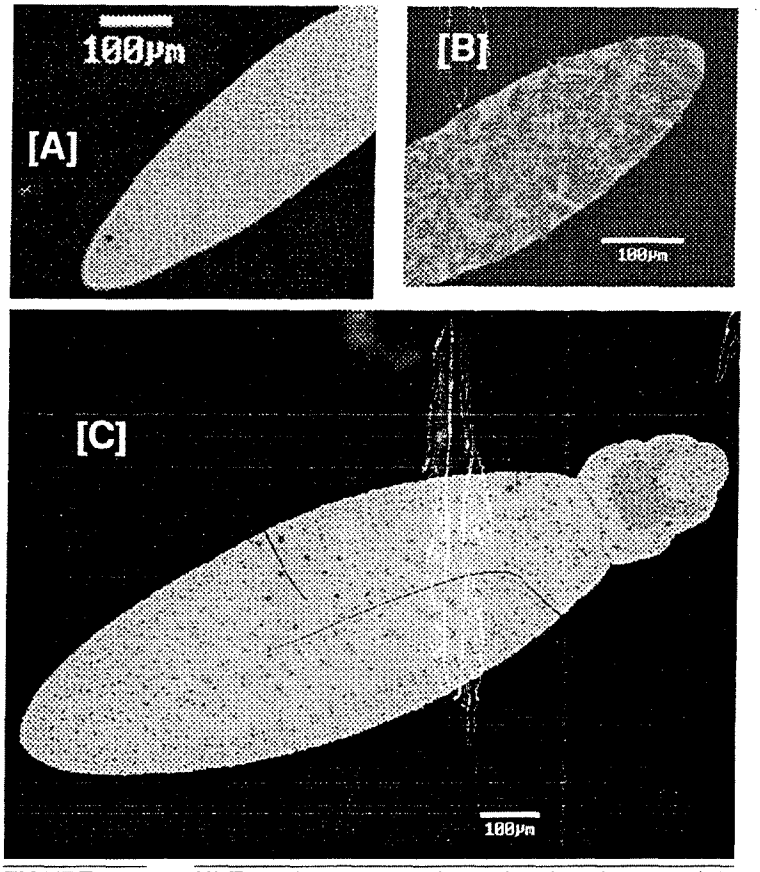

FIGURE 6. Ni-Fe rods cross-sections showing the sample's microstructure. All rods were grown at 20mbar partial pressure of $Fe(CO)_5$ and at laser power of 190mWatts. The respective precursor and deposit concentrations are reported below.

Sample	Gas Mixture		Deposit Composition	
	$Fe(CO)_5$ Conc. (%)	Ni(CO)4 Conc. (%)	Fe Conc. (%)	Ni Conc. (%)
A	50.0	50.0	52.0	48.0
B	42.0	58.0	29.0	71.0
C	55.6	44.4	48.0	52.0

Figure 5 displays measurements of length over time for a typical rod, as well as the diameter of the rod during the same time period (820 s). One can see that the axial rate rises rapidly to the steady-state growth rate (indicated by the slope of the solid line), and then the axial rate slows to a new terminal rate, Rt. At the same time, the rod diameter at mid-length grows steadily, beginning at 250 mm, ultimately reaching over 1000 mm in diameter. Perhaps the most significant result from this figure is that, while the steady-state axial rate greatly exceeds the radial rate (hence the rod), the terminal rate, Rt, and the radial rate are nearly the same. Consequently, for metals under a de-focused beam, the entire rod grows at a uniform rate, and the temperature gradient along the rod is small.

Fig. 2 Ni-Fe atomic ratio vs. $Fe(CO)_5$ and $Ni(CO)_4$ gas concentrations.

● Auger

⊘ Microprobe

Beam Power=300 mW (Wo=25μm).

Total Pressure=20-48 mbar.

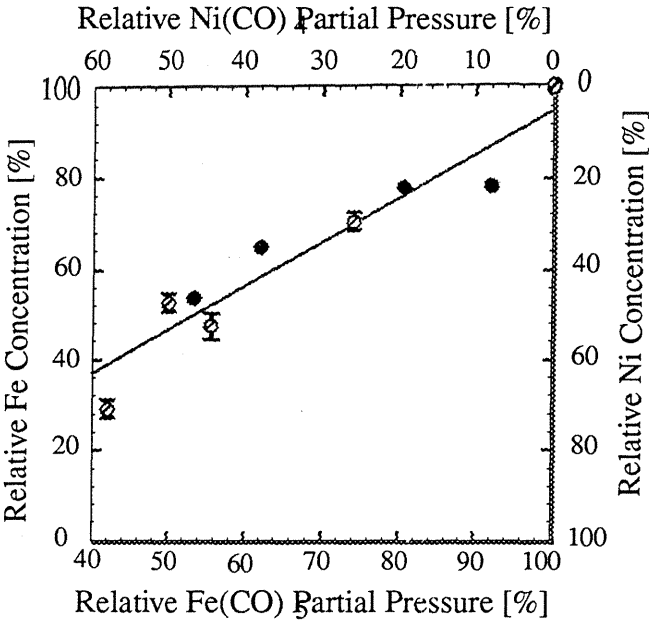

FIGURE 7. Rod composition vs. gas mixture composition for Auger and Microprobe measurements.

3.2 NI-FE GROWTH

Sample structures were grown from various precursor mixtures of Nickel and Iron carbonyls. The sample composition was shown to vary with the precursor partial pressures and demonstrated the capability for alloying as well as fabricating functionally graded materials.

Alloy Composition: Figure 6 shows the cross-section and microstructure of several rods grown at the same incident power, but differing precursor concentrations. The Fe(CO)5 precursor partial pressure in Figure 6.B is the lowest of the three cases (42%); the Fe(CO)5 pressure increases in the case of Figure 6.B to 50%, and reaches its maximum value at 55.6% in Figure 6.C.

Throughout each sample, the ratio of Ni-Fe (in at.%) remained nearly constant due to the large capacity of the reactor chamber. The samples exhibited regions that were heavily oxidized regions, and, in the case of Figure 6.B, inclusion of graphitic flakes. Yet the relative composition of the deposit remains constant to within ±2 percent. Figure 7 summarizes the final composition of the Ni-Fe rods versus the gas mixture in which they were grown. The partial pressures of Ni(CO)4 and Fe(CO)5 were varied as a percentage of the total chamber pressure, giving rods of similar atomic Ni-Fe ratios. In all cases, the chamber was filled with Fe(CO)5 to 20 mbar, and Ni(CO)4 was added to give a specific relative gas concentration. It is apparent that any Ni-Fe alloy may be produced in this manner, including high-temperature super-alloys with Ni concentrations greater than 25%.

3.3 VOLUMETRIC GROWTH RATE MEASUREMENT

Growth Rate Measure: Using a stationary beam with focus at the substrate, straight-sided needles of graphite, nickel, iron, and nickel-iron alloys up to 7 mm in length could be deposited without moving the laser focus. Note that this is many times the diffraction-limited Rayleigh Range of the beam focus (260 μm).

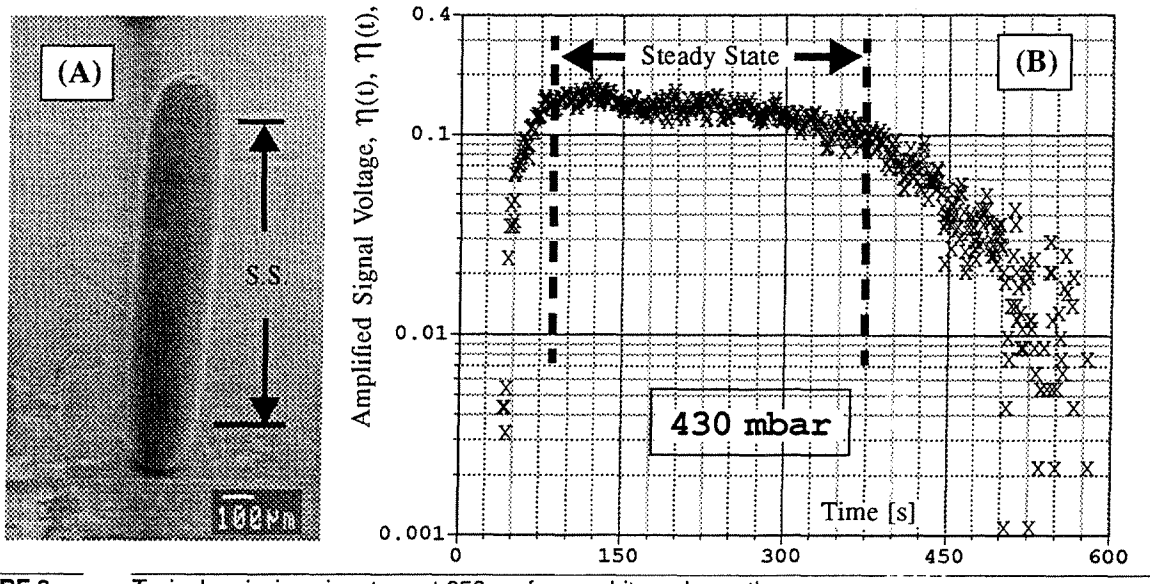

FIGURE 8. Typical emission signature at 656nm for graphite rod growth.

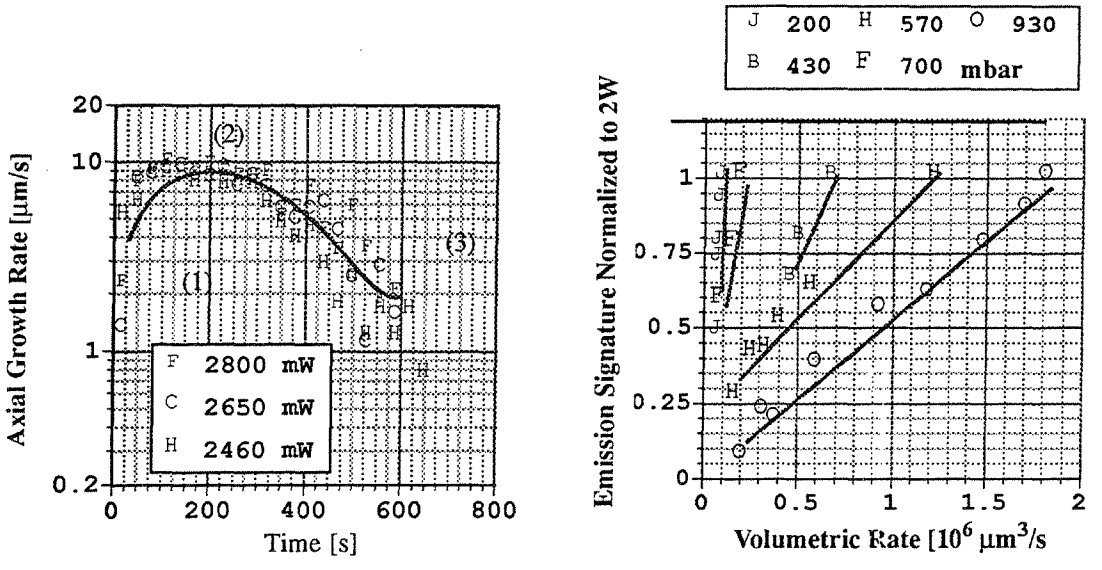

FIGURE 9. Correlation of emission signature to volumetric growth rate for graphite rod growth.

The normal deposition rate, Rn, of rods deposited in this manner is defined as the local rate at any surface point where growth occurs. The axial deposition rate, Ro, is the normal growth rate at the center of the rod, along the beam axis. The final radius of a rod, Rs, can be estimated at any axial point by integrating the component of the normal deposition rate perpendicular to the beam axis over time. The volumetric deposition rate, Rv, of a *cylindrical rod* depends on both the axial rate and diameter deposited over time.The normal rate, Rn, varies exponentially with laser power in the kinetic regime, while at high incident powers, it may become transport limited.

Growth Regimes. Figure 8 shows the emission signature vs. time for a typical graphite rod. Figure 9 correlates the emission signature to the volumetric growth rate. After a brief delay, representative of thin film nucleation and coalescence at the substrate, rapid axial growth commences, eventually rising to a peak rate. This interval is denoted the transient regime,

labeled (1) in Figure 9. Once the peak rate is attained, the rod grows at a constant axial rate, and it is over this steady-state regime —labeled (2) in Figure 9— that the bulk of the rod is grown. Eventually, (at approximately 300 seconds, labeled (3) in Figure 9) the axial rate slows, dropping linearly as the beam broadens and the surface temperature decreases; this is known as the tail regime.

Volumetric Rate Measure. Emission spectra produced during the pyrolytic decomposition of ethylene were monitored using the photodetector and filters described previously. The hydrogen-Alpha line at 656 nm was found to be several orders of magnitude brighter than the background thermal emissions. This spectral line represents the n=3 --> n=2 transition in the Balmer Series of atomic hydrogen, as occurs following disassociation of hydrogen from C_2H_4 as well as from the thermal ionization of H_2. Since ethylene dissociates at a lower temperature than the ionization potential of hydrogen, the measured emission spectra were primarily due to the liberation of atomic hydrogen during pyrolysis of C_2H_4.

Since the signal strength is proportional to the total number of disassociated hydrogen ions returning to the ground state, it was hypothesized that the emission signature is representative of the volumetric deposition rate. This was confirmed by Figure 9, where the steady-state signal amplitude is plotted vs. measured volumetric rate along lines of constant pressure. Each curve is normalized to the amplitude of the emission at incident powers of 2000 mW. Observe that in each case, the signal strength is linearly proportional to the volumetric rate. When sufficiently well calibrated for the precursor partial pressure and viewing position, the signal amplitude can be used as an absolute measure of volumetric rate.

3.4 AXI-SYMMETRIC CONTROL OF 3D-LCVD

The one-to-one correspondence of volumetric rate and radius (at any given pressure) makes it possible to create a very stable controller for 3D-LCVD. If the spectral emission signature is fed back to the laser power controller, and compensation is made in the laser power to obtain a desired volumetric growth rate, one obtains direct control over the axi-symmetric 3D-LCVD process. Proportional-derivative-integral (PID) control was used to set the laser power in real-time with feedback from the emission signature.

To demonstrate, a series of samples were grown in this manner, such as the structures shown in Figure 10. All samples were grown at 200 mbar, so that the axial rate would be transport limited and to allow sufficient time for the controller to respond to the growth. (At 930 mbar, rods grow so rapidly that the steady-state regime passes in just a few seconds.) The laser power was set at maximum power to initiate growth on the graphite substrate through the transient regime. The feedback controller was then engaged after the rods had reached their steady-state radius (labelled 1 in Figure 10.A. The sample in Figure 10.A was grown using a linearly decreasing setpoint over the length labelled (2), while the sample in (B) was grown with an exponentially decaying total laser power in place of the PID control.

The most promising feature of this control technique is that the output shape is similar to the input waveform; the linear setpoint decay in (A) resulted in a straight cone, while the sinusoidal growth input in (C) resulted in periodic bulbs. The opposite is true for open-loop laser power control, where an exponential decay in the power is required to produce a linearly tapered rod.

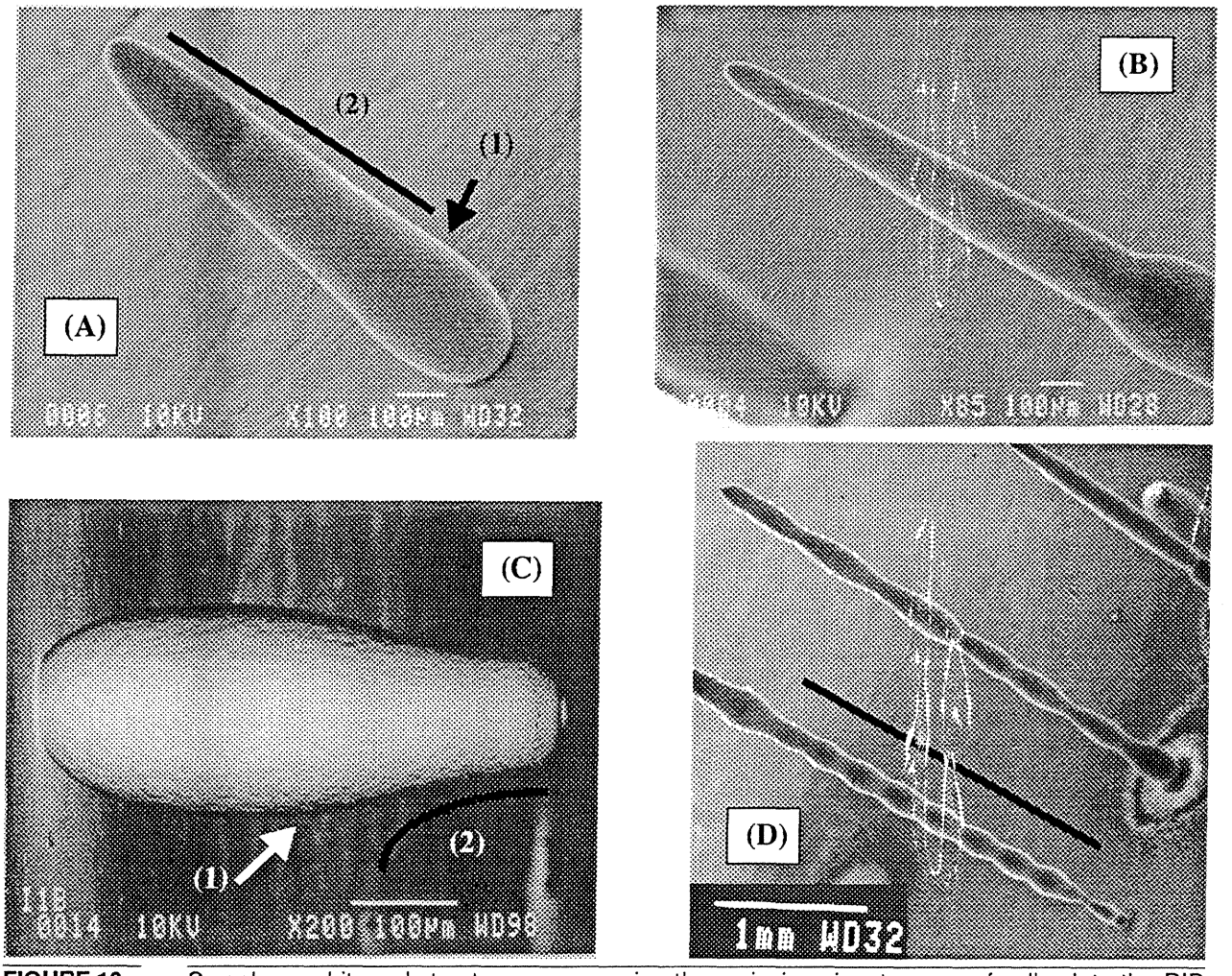

FIGURE 10. Sample graphite rod structures grown using the emission signature as a feedback to the PID controller.

3.5 GRAPHITE TEMPERATURE MEASUREMENTS

Temperature Gradient Measurements: In this section, the temperature gradient over several graphite rods will be measured from the blackbody radiation emitted during their growth. Kodak High Speed infrared emulsion no. 2681 was employed throughout the experiments. A standard 250 mm telephoto lens was used in combination with a 250 mm achromat, achieving a 1.2x magnification of the object on the film. Exposures were made at various wavelengths using narrow--band filters.

Temperature Measurements: Figure 11 displays several successive photographs of the same rod taken at various wavelengths; the frames were taken during the steady-state growth regime in rapid succession. The rods were viewed at a 45±1° angle from the laser axis. The resolution of the photographs is approximately 7 μm, and the direction of the incident beam is shown by the dashed, blue arrows. The brightest regions are the surface of the rod; these are color-coded red, orange, and yellow, in descending intensity according to the color bar. The gas surrounding the rods also emits weakly, and this appears primarily as green, blue, and purple surrounding the brighter regions.

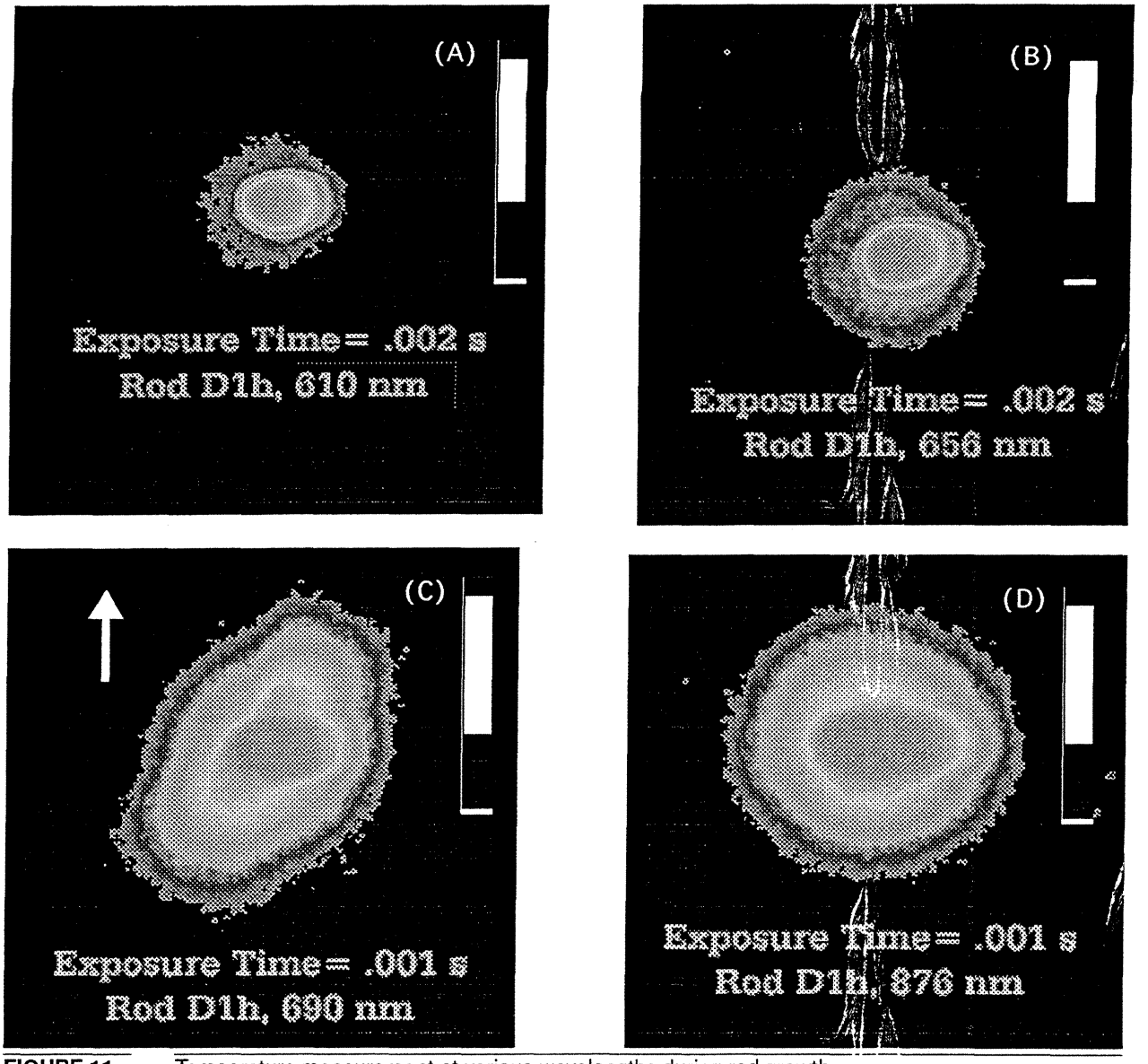

FIGURE 11. Temperature measurement at various wavelengths during rod growth.

Finally for the rod grown at 2930 mW, the power is sufficient at the tip to reach graphite's sublimation temperature of 3925 K; in fact, SEM photos of this rod exhibit slight dimpling, such as found more prominently on rods grown at higher laser powers–and previously attributed to mass transport limitation. A slight warpage near the rod tip is also visible, possibly due to softening of the graphite at excessive temperature. It remains to be seen if the dimple effect is entirely caused by diffusion limitation, sublimation, or a combination of both phenomena.

4 CONCLUSIONS

Controlled 3-dimensional laser-induced vapor deposition of Ni-Fe alloys is feasible from nickel and iron carbonyls, producing alloys with less than ±2 at.% compositional variance. Sustainable steady-state growth rates of up to 30μm/s are possible. Further studies will determine the detailed microstructure and hardness of the Ni-Fe deposits, as well as the activation energy of $Fe(CO)_5$.

In addition to controlling the laser power, the emission signature could also be used for focal positioning, comparing the actual emission amplitudes with the expected steady-state rates, compensating to maintain the steady-state focal position.

Direct feedback control of the growth rate will also be essential for layered growth, as previous attempts to build-up shapes by repetitive scanning have proven to be unstable. As one layer is grown over another using open-loop control, perturbations in the thickness of the underlying deposit induce exponential perturbations in the next layer (kinetic regime), yielding irregular deposits. With growth rate control, compensation can be made for such perturbations, and rate-controlled 3D-LCVD can be used for both layered and continuous growth.

Similarly, the growth control method could be used to obtain consistent direct writing results over varying topographies and substrate materials.

5 ACKNOWLEDGEMENTS

The authors wish to thank the National Science Foundation (Grants: NSF ECS-9314071 and NSF DDM-9057059) for their generous support. Grateful acknowledgments also go to Ray Dove of the Rensselaer MRC microscopy laboratory for the SEM photos, Dr. Hudson of the Rensselaer Materials Engineering Department, for use of the Auger Microprobe, Norm Gendron, of Rensselaer, for advice in sectioning the samples, and David Wark of the Rensselaer Geology Dept. for contributing to the x-ray microprobe analysis. Thanks finally to the CIEEM staff for helping to dispose of the iron and nickel carbonyls.

6 REFERENCES

[Bäuerle, 1984] D. Bäuerle, Laser Processing and Diagnostics, Springer Ser. in Chem. Phys., 39, 166-182.

[Zong, 1992] G.-S. Zong, Ph.D. Thesis, University of Texas at Austin, Department of Materials Science.

[Westberg et al., 1993] Westberg, H., Boman, M., Johansson, S., Schweitz, J.-A., J. Appl. Phys., 73, 7864-7871.

[Maxwell et al., 1993] J.L. Maxwell, J. Pegna, and A. Ostrogorski, Proc. Solid Freeform Fabrication Symposium, Austin, TX, 253-271.

[Lehmann et al., 1991] Lehmann, O., Stuke, M., Applied Physics A, 53, 343-345.

[Wallenberger et al., 1993] F.T. Wallenberger, P.C. Nordine, Science, 260, 66-68.

[Wallenberger et al., 1992] Wallenberger, F. T., Nordine, P. C., Materials Letters, 14, 198-202.

[Rytz-Froidevaux et al., 1981] Rytz-Froidevaux, Y., Salathé, R. P., Gilgen, H. H., Physics Letters, 84A, 216-218 (1981)

[Arnone et al., 1986] Arnone, C., Rothschild, M., Black, J. G., Ehrlich, D. J., Appl. Phys. Lett., 48, 1018-1020.

[Maxwell et al., 1995] J.L. Maxwell, J. Pegna and E. Hill, Proc. Solid Freeform Fabrication Symposium, Austin, TX, 143-150.

[Bäuerle, 1986] D. Bäuerle, Chemical Processing with Lasers, Springer-Verlag, NY, 93 (1986).

[Maxwell et al., 1996] J.L. Maxwell, J. Pegna and D. Messia, Real Time Growth Rate Measurements and Feedback Control of Three-Dimensional Laser Chemical Vapor Deposition, Submitted to Applied Physics A.

[Touloukian, 1970] Y.S. Touloukian, Thermophysical Properties of Matter, 1, IFI/Plenum, NY.
[Armstrong et al., 1990] Armstrong, J. V., Enrech, M., Decrouez, C., Lunney, J. G., Coey, J. M. D., IEEE Transactions on Magnetics, 26, 1629-1631.
[Garrett et al., 1934] A.P. Garrett, H.W. Thompson, J. Chem. Soc., 1817 (1934).